

NMR study of translational and rotational dynamics in monoolein-water mesophases: Obstruction and hydration effects

Thorsten Feiweier,^{1,2} Burkhard Geil,^{1,3} Eva-Maria Pospiech,⁴ Franz Fujara,^{1,3} and Roland Winter⁴

¹Fachbereich Physik, Universität Dortmund, D-44221 Dortmund, Germany

²Siemens AG, D-91058 Erlangen, Germany

³Fachbereich Physik, TU Darmstadt, D-64289 Darmstadt, Germany

⁴Fachbereich Chemie, Universität Dortmund, D-44221 Dortmund, Germany

(Received 24 May 2000)

Using a variety of NMR methods (magnetic field gradient echo decays, ²H one- and two-dimensional spectra, spin-lattice relaxation rates), both translational and rotational dynamics of the constituents of monoolein MO/H₂O mesophases have been studied. The experiments lead to the following conclusions. The translational dynamics of the lipid molecules is essentially dominated by obstruction effects due to the topologies of the diverse mesophases. On the other hand, water dynamics—in the regime of small water concentrations—is strongly influenced by hydration of the lipid head groups. Hydration is seen in diffusion data, in spectra and in spin-lattice relaxation of the water molecules. This work represents an involved extension of our recently published work [Chem. Phys. Lipids **106**, 115 (2000)].

PACS number(s): 68.45.Kg, 76.60.-k, 87.15.-v

I. INTRODUCTION

In a recent paper [1], we studied the temperature dependence of the translational diffusion of the neutral amphiphilic molecule monoolein (MO) and water in solutions of varying water content. Although most lipids in excess water exist in lamellar bilayer phases, certain lipids, including monoacylglycerides, can form a nonbilayer hexagonal (H_{II}) and/or cubic liquid-crystalline phases as well. Most of the cubic liquid-crystalline phases are now known to consist of bicontinuous regions of water and hydrocarbon, which can be described by infinite periodic minimal surfaces (IPMS's). An IPMS is an intersection-free surface periodic in three dimensions with a mean curvature that is everywhere zero. The surface, formed by the lipid bilayer midplane, separates two interpenetrating but not connected water networks. Nonlamellar phases, which occur for a number of membrane lipids, probably play an important functional role in some cell processes as local and transient intermediates. For example, cubic structures seem to be involved in membrane fusion and fat digestion, and might occur in intracellular organelles. There is also considerable evidence that microorganisms control the lipid composition of their membranes so as to maintain them close to a composition where nonlamellar structures would begin to appear. The monoacylglyceride 1-monoolein (C18:1c9, Fig. 1) was chosen for investigation because it exhibits mesomorphic phases with different lattice dimensionality at different levels of hydration and at rather moderate conditions of temperature and pressure. Furthermore, its physicochemical properties have received considerable interest due to their importance as intermediates in fat digestion and metabolism, and because of their applications in the food industry. It is a neutral lipid and the *cis* double bond of MO is located at the 9, 10 position of its acyl chain. The temperature-water concentration phase diagrams of MO have been established by several authors [2,3,4] (Fig. 1).

In our studies we use deuterated water, which enables us

to look at lipid diffusion (¹H-NMR) and at water diffusion (²H-NMR) using the very same samples. The results obtained in our previous work [1] may be briefly reviewed as follows.

(1) By applying static magnetic field gradient ¹H-NMR, we see the lipid diffusion in the two cubic phases Q_{II}^G and Q_{II}^D and in the inverse hexagonal phase H_{II}. The “effective” diffusion coefficient D_{eff} reflects the local mesophase topology (obstruction effect). It is found that the transition between the two cubic phases does not alter the obstruction factor, while the transition from the cubic to the H_{II} phase significantly reduces D_{eff} .

(2) In the cubic phases, the diffusion time independence of the ¹H echo decays is consistent with the isotropicity of these phases on length scales comparable to the diffusion length.

(3) In the inverse hexagonal phase, the time dependence of the ¹H decay behavior is very weak. This can only be understood by assuming a value of less than about 1 μm for the upper limit of the correlation length of the tube director.

(4) The analysis of the ²H gradient NMR echo decay curves reveals the existence of two deuteron species. A com-

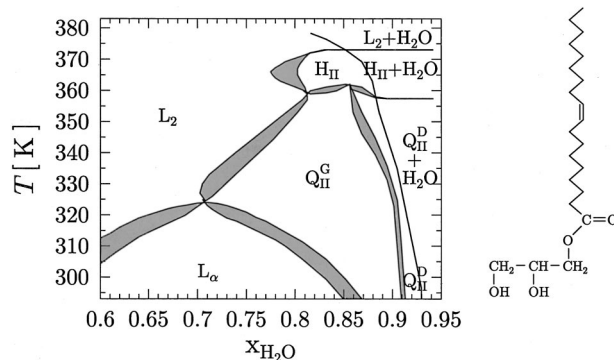


FIG. 1. Monoolein (right) and phase diagram (left) of the MO/H₂O system after Hyde and Anderson [2].

parative ^{17}O NMR study proves that this is *not* due to two water species but rather caused by a slow exchange (on a time scale of a few ms) of the deuterons between the water and the lipid headgroup. Application of an exchange model quantifies the deuteron residence time in the water phase and the effective water diffusivity.

(5) The effective water diffusion coefficient (fast component of the ^2H echo decay curves) is reduced by roughly an order of magnitude as compared to that of bulk water, which cannot be explained by pure obstruction effects.

These results represent the starting point for our present study. In summing up once again, our NMR probe, which studies the lipid and water *translational* dynamics over a mesoscopic length scale, has been indicative of the characteristic structure-dynamics relationships expected in these mesomorphs. However, a few open questions as addressed above need further consideration. These questions have been further pursued by ^2H NMR spectroscopic experiments on water in the same samples as those used in our preceding study. The experiments lead us to the present paper, which is organized in the following way. We start with a review of what can theoretically be expected from the diverse ^2H NMR methods involving water in lyotropic phases (Sec. II). Then, we turn to the presentation of our new experimental results. Here, we first discuss one-dimensional (1D) and two-dimensional ^2H NMR spectra which we measured with the goal of getting information on the water *rotational* dynamics (Sec. III A). Although this kind of spectroscopy is usually considered a local probe, we already anticipate at this point that in our structured mesophases the experiments will yield information about dynamical processes over length scales comparable to those studied by gradient NMR. A second motivation for our present work has been our desire to compare, as far as the water dynamics is concerned, translation and rotation. Such a comparison will shed new light on our previous diffusion results [1]. Another kind of experiment requires spin-lattice relaxation rates as a true local probe (Sec. III B). We then turn to a concerted discussion of all three observables, (i) diffusion, (ii) spectral line shapes, and (iii) spin-lattice relaxation rates in terms of obstruction (Sec. IV A) and hydration (Sec. IV B) effects. Finally, we present our conclusion (Sec. V) and a summary of open questions, which call for further investigations (Sec. VI).

II. METHODS

In our previous paper [1], we essentially concentrated on NMR echo decays in a static magnetic field gradient yielding information on lipid (^1H NMR) and water (^2H NMR) diffusion. We will not go into the experimental details, although we will raise all of those results again for a more elaborate discussion (Sec. IV). Here, we add results on ^2H free-induction decay (FID) spectra and spin-lattice relaxation rates on (deuterated) water, both 1D and 2D. The hardware used for these experiments consists of an 8.5 T cryomagnet and a homemade dedicated single-channel, high-power, spectrometer running at a ^2H NMR frequency of about 55 MHz. Further, lipid ^1H relaxation rates have been obtained in parallel with our previous [1] diffusion data; for details of the ^1H data, see also Sec. III B below. Great care has been taken with the sample temperature variation and control by

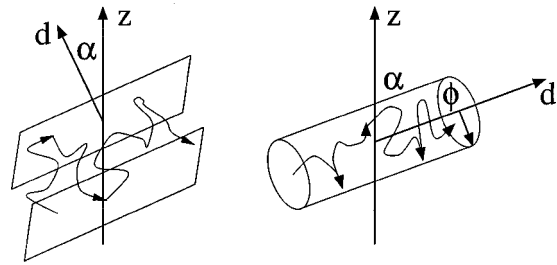


FIG. 2. Schematic representation of a lamellar (left) and a hexagonal (right) phase. The polar angle α is defined by the z axis (in the laboratory frame) and the director \vec{d} . The path of a water molecule is indicated.

using a commercial flow cryostat. In the following, some basic information on the wealth of ^2H NMR spectroscopy in our context is given.

A. One-dimensional (1D) ^2H FID spectra on water in lyotropic phases

The essential feature of ^2H NMR spectroscopy is the existence of a quadrupole frequency

$$\omega_Q(\theta) = \delta(3 \cos^2 \theta - 1) \quad (1)$$

with—to a very good approximation for a C- ^2H bond and still reasonably approximative in the case of an O- ^2H (e.g., water [5])— θ denoting the orientation of the tagged bond direction with respect to that of the external magnetic field. The quadrupole frequency adds to and subtracts from the Zeeman frequency ω_Z , yielding a two-line spectrum at frequencies

$$\omega(\theta) = \omega_Z \pm \omega_Q(\theta) = \omega_Z \pm \delta(3 \cos^2 \theta - 1). \quad (2)$$

δ denotes the strength of the electric quadrupole interaction. In the case of solid powders (e.g., ice) the inhomogeneous average due to all bond orientations leads to the famous Pake spectrum with a frequency width between the two “singularities” of more than 100 kHz. In the presence of molecular motion, it is well known [6] that 1D ^2H spectra contain information on the residual orientation $\langle \theta \rangle_\tau$ which averages over the history of orientations of the considered bond within the FID duration τ . The best known case of dynamical averaging is that of isotropic reorientation in a bulk liquid. Seeking the angular probability distribution of meeting an orientation θ , we arrive in this case at a probability density $P(\cos \theta) = \text{const}$. In a fast motional limit (“extreme motional narrowing”), this implies an average resonance frequency

$$\langle \omega \rangle_\tau = \int_{-1}^{+1} d \cos \theta \omega_Q(\theta) P(\cos \theta). \quad (3)$$

Let us now look at liquid molecules intercalated between two parallel surfaces, as in the case for water in the lamellar phase (Fig. 2, left). Near the lipid surface a water molecule is expected to be aligned relative to the membrane director (hydration). If we assume that fast local rotational dynamics of hydrated water only partially averages over all possible quadrupolar frequencies and that, due to the symmetry of the

topology, the principal axis of the residual anisotropy tensor points toward the director, we are led to a probability density

$$P(\cos \theta) = c[p \delta_{(\cos \theta - \cos \alpha)} + (1-p)]. \quad (4)$$

Here, p denotes the excess probability of an orientation parallel to the director and thereby accounts for the local anisotropic dynamics; δ_{index} is the Kronecker symbol, and c normalizes the probability density. From Eq. (4) we obtain the dependence of the averaged resonance frequency on the angle α between the director and the external magnetic field,

$$\langle \omega(\alpha) \rangle_{\tau} = \omega_Z \pm \frac{1}{2} p \delta (3 \cos^2 \alpha - 1). \quad (5)$$

A comparison with Eq. (2) indicates that in case of a powder average of the director we will again get a Pake spectrum, the width of which is reduced by a factor $S = \frac{1}{2} p = \frac{1}{2} \langle (3 \cos^2 \theta - 1) \rangle_{\tau}$ as compared to that of a rigid powder. S is often identified with an order parameter of the intercalated water molecules [7].

In the hexagonal phase, the line shape is derived in an analogous way, except that we now deal with a somewhat more involved geometry (Fig. 2, right):

$$P(\cos \theta) = c \left[\frac{p}{2\pi} \int_0^{2\pi} d\Phi \delta_{(\cos \theta - \cos \phi \sin \alpha)} + (1-p) \right]. \quad (6)$$

The residual principal axis now points radially out from the cylinder, i.e., it is oriented perpendicularly to the director with an azimuthal angle ϕ . The temporal average is then calculated as

$$\langle \omega(\alpha) \rangle_{\tau} = \omega_Z \pm \frac{p}{2} \delta (3 \cos^2 \alpha - 1). \quad (7)$$

This is the same result as that for the case of a lamellar phase [Eq. (5)] except for another width reduction by a factor of 2 [8]. Note that to obtain this straightforward result, we have assumed that the local dynamics and the degree of hydration are identical in both the lamellar and hexagonal phases.

In the case of cubic topologies, no direction is preferred. As long as the diffusion length within the time interval τ exceeds the elementary cell size, the water dynamics can be considered to be isotropic. In consequence, we expect, just as in the bulk case, a narrow line at $\omega = \omega_Z$.

B. Two-dimensional ^2H echo exchange spectroscopy

Starting off with basically a three-pulse stimulated echo experiment, (pulse)- τ_1 -(pulse)- t -(pulse)- τ_2 -echo, we measure a tagged particle correlation function [6]

$$S(\tau_1, \tau_2; t) = \langle e^{-i\omega_Q(0)\tau_1} e^{+i\omega_Q(t)\tau_2} \rangle, \quad (8)$$

the double Fourier transform \mathcal{F} of which

$$S(\omega_Q(0), \omega_Q(t)) = \mathcal{F}[\mathcal{F}(S(\tau_1, \tau_2; t))_{\tau_1}]_{\tau_2} \quad (9)$$

is the so-called 2D-exchange spectrum. 2D spectra are interpreted as follows. The intensity at the coordinate $[\omega_Q(0), \omega_Q(t)]$ stems from deuterons, the resonance frequencies of which are determined before and after the mix-

ing time t by principal axis orientations $\theta(0)$ and $\theta(t)$, respectively. For $t \rightarrow 0$ or in the absence of molecular reorientations, we expect intensity exclusively at the diagonal. For increasing t there will be a gradual increase (described by some correlation time) of nondiagonal intensity, the pattern of which will be indicative of the geometry of molecular reorientations. For instance, two important limiting “types” of isotropic reorientations, rotational diffusion and random jumps, can be clearly distinguished from each other [9,10].

At this point we wish to comment, most importantly for the sake of our present context, i.e., in the presence of confined geometries, on the enormously rich potential of 2D spectroscopy with some general considerations. Just as 1D spectra of confined and/or intercalated water should no longer be regarded as the powder average of the water molecules but rather as the powder average of the directors (cf. discussion in Sec. II A), 2D spectra also inform us about reorientations of the residual principal axes. To be more specific, let us consider the lamellar phase. The occurrence of nondiagonal intensity could be interpreted in several ways: (i) by assuming the presence of water molecules that follow a reorientational dynamics of the lamella as a whole; (ii) by assuming the occurrence of long-range water diffusion that passes several lamellar crystallites; or (iii) by assuming the diffusion of water molecules along curved (static) lamellar surfaces (e.g., in the interlamellar water layers of multilamellar vesicles). Case (ii), where the director orientations of adjacent stacks of lamellae are expected to be uncorrelated, would appear as an apparent random jump process. From the correlation time and the (known) diffusion constant, we could infer the domain size. For spherical vesicles, case (iii) implies rotational diffusion of the water molecules, and analysis of the 2D spectra would yield an estimate of the mean vesicle diameter.

C. Samples

For most details of the sample preparation and characterization, we refer to our previous paper [1]. Here, we add a few but very important remarks on the sample systematics since in the present work we will use the degree of hydration as an important parameter. The set of studied $\text{MO}^2\text{H}_2\text{O}$ samples consists of two batches, prepared in different ways. Table I shows all samples and their compositions.

For batch 1 the desired amounts of the two components are weighed and mixed/homogenized *outside* the NMR sample tube as described in Ref. [1]. The preparation of the batch 2 samples differ in that the two components are put into the sample tube, which is then sealed, before homogenization. Mixing/homogenization of the dispersion already *inside* the NMR tube is performed essentially by centrifuge treatment and freeze-thaw cycles. An *a posteriori* comparison of the two procedures favors the second one, since it avoids homogenization under less precise open-air conditions. However, even if a slight uncertainty in the water content cannot thereby be excluded, we estimate the precision of the water content to 2–3 wt%. The samples prepared with $^2\text{H}_2\text{O}$ have been compared with samples of equal water concentration but prepared with H_2O by differential scanning calorimetry and small-angle x-ray scattering [1] to check for

TABLE I. Composition of the samples studied. The water is deuterated. Exception: Sample no. 11 contains 13 wt % ^{17}O -enriched water and 10 wt % $^2\text{H}_2\text{O}$.

Sample no.	Batch	wt % water	x_{water}	$n_{\text{water}}/n_{\text{lipid}}$
1	1	14	0.74	2.85
2	1	19	0.81	4.26
3	1	23	0.84	5.25
4	1	26	0.86	6.14
5	1	39	0.92	11.5
6	2	18	0.80	4.00
7	2	22	0.83	4.88
8	2	24	0.85	5.67
9	2	28	0.87	6.69
10	2	35	0.91	10.1
11	2	23	0.84	5.25

isotopic effects. No significant difference between the phase transition temperatures of the systems $\text{MO}/^2\text{H}_2\text{O}$ and $\text{MO}/\text{H}_2\text{O}$ are observed within the accuracy of our measurements.

III. EXPERIMENT RESULTS

A. Water rotational dynamics

1. 1D spectra

Let us begin by presenting in Fig. 3(a) a typical set of ^2H 1D echo spectra as obtained from one of the MO/water samples (sample no. 3). This figure contains plenty of valuable information. We immediately note from inspection of the figure that at least qualitatively our expectations discussed in Sec. II A are fulfilled: At low T (lamellar phase) we find a Pake spectrum, at intermediate T (cubic phase) the line is isotropically narrowed, at high T (hexagonal phase) a Pake spectrum reappears. The widths of the anisotropic spectra are reduced by roughly two orders of magnitude with respect to static solid state spectra, which may be expressed by an order parameter of about 0.01 [cf. Eq. (5)]. Further, the width of the hexagonal phase spectra is reduced as compared to that of the lamellar phase spectra. However, instead of the expected factor of $\frac{1}{2}$ [Eq. (7)], we observe a ratio (width in the hexagonal phase versus width in the lamellar phase) of about 0.36. This may be due to deviations from simple tubular H_{II} topology or to an increased lipid head group dynamics in the high-temperature phase leading to a reduced order parameter. Finally, we note that the transition temperatures $T(L_{\alpha} \rightarrow Q_{\text{II}}^{\text{G}})$ and $T(Q_{\text{II}}^{\text{G}} \rightarrow \text{H}_{\text{II}})$, although experimentally precisely determined within ± 1 K, differ considerably from those in Fig. 1.

A closer look at the lamellar phase spectrum reveals the existence of another weak Pake type spectral contribution, the singularities of which are indicated by the arrows in Fig. 3(b). The width of this spectrum is quantified by assigning a quadrupole coupling constant about three times larger to a small contribution of less mobile deuterons, i.e., less preaveraged $\text{O}-^2\text{H}$ bond orientations. On the time scale of the experiment (inverse coupling constant ≈ 1 ms) there is no exchange between the two species. Undoubtedly, the “weak” species is to be identified with those deuterons which, ac-

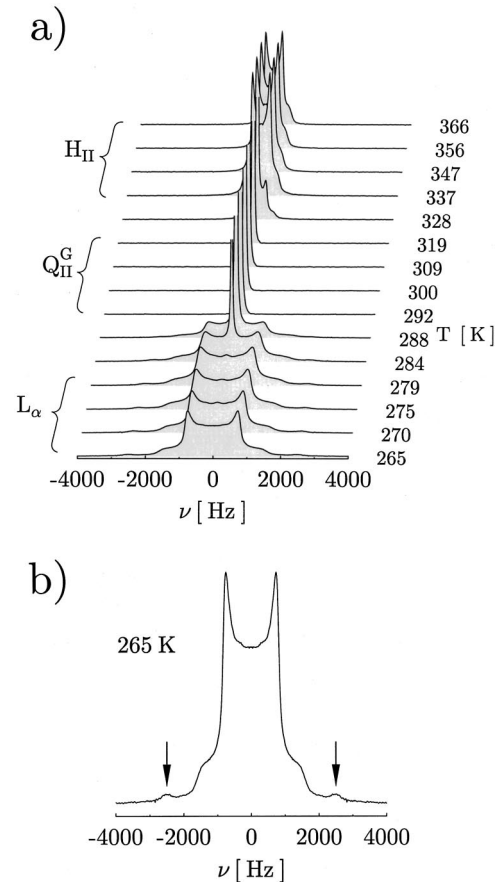


FIG. 3. (a) A series of deuterium FID spectra taken from sample no. 3 ($\text{MO}/23$ wt% $^2\text{H}_2\text{O}$) at different temperatures. (b) A more detailed look at the spectrum obtained at 265 K. Arrows mark the singularities of a weak second contribution; see text.

ording to our earlier diffusion data in the cubic phases [1], are chemically attached to the lipid headgroups. This interpretation is also consistent with high-resolution ^1H spectra [11]. If we compare the ratio of the integrated intensities of the two subspectra with the (number) ratio of deuterons at the two sites as expected from the sample preparations, we find an agreement within a factor of about 1.5. In contrast to the lamellar phase, the hexagonal-phase spectra do not show comparable weak wings, which is indicative of an increased exchange rate leading to homogeneously averaged spectra.

Except for the lowest hydrated sample (no. 1), with 14 wt% $^2\text{H}_2\text{O}$, the residual quadrupole coupling constants of water in the lamellar phase always slightly *increase* with temperature. In contrast, that of the lipid headgroup deuterons decreases (Fig. 4). There are two mechanisms which could qualitatively explain such a behavior. Increased deuterium exchange rates may gradually fall into the FID dynamic range, thus causing the Pake spectra singularities to move toward each other. In addition, with increasing temperature the lipid headgroup subspectrum will get narrower due to a more pronounced headgroup local dynamics. Such a behavior is well known from infrared spectroscopy studies [12]. This could then also nicely explain the exceptional decrease of $\Delta\nu_Q$ of the water subspectrum in sample no. 1, where the water concentration is low enough that most water molecules are subjected to the lipid headgroup dynamics. In

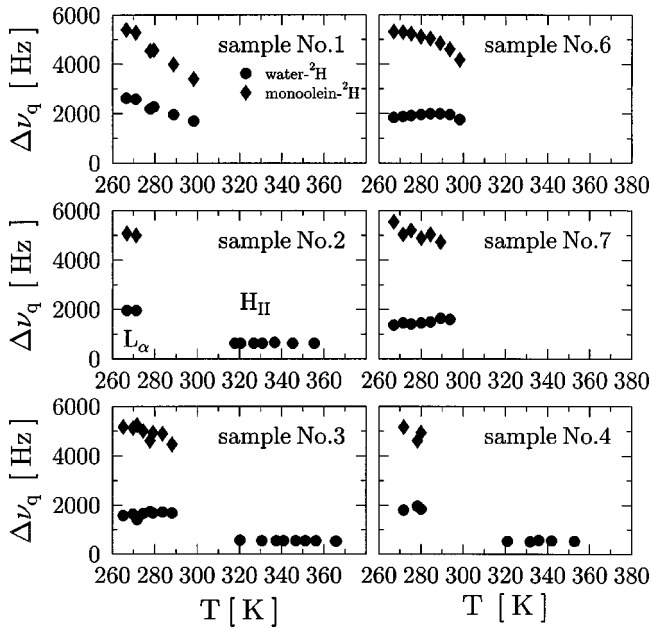


FIG. 4. Temperature dependence of the residual coupling constants in the lamellar and hexagonal phases of MO/ $^2\text{H}_2\text{O}$. The level of hydration increases from upper left to lower right.

Sec. V, we will revisit this latter point in the context of a layered hydration model.

2. 2D spectra

The question of what kind of dynamics takes place at time scales above the one which is accessible with 1D spectra is answered by 2D NMR exchange spectra. In the following, we will therefore reconsider three cases where anisotropic ^2H spectra have been found—the lamellar phase, the lamellar/cubic two-phase region, and the hexagonal phase—and proceed with the discussion of 2D spectra.

Let us start with a series of spectra taken in the lamellar L_α phase (Fig. 5). At the shortest t value the intensity is found at the principal diagonal axis and the line shape corresponds to the 1D spectrum as described above. Again, the narrow line width indicates that the Pake pattern is formed by a powder average over the membrane directors. Individual molecular rotations are already averaged out on the time scale of a few hundred μs . And also again we observe a two-component spectrum. The singularities arising from the lipid headgroup deuterons are clearly visible in the outer diagonal part of the spectrum. With increasing t , the intensity flows into the off-diagonal parts of the spectrum forming characteristic box-shaped patterns known from diffusional

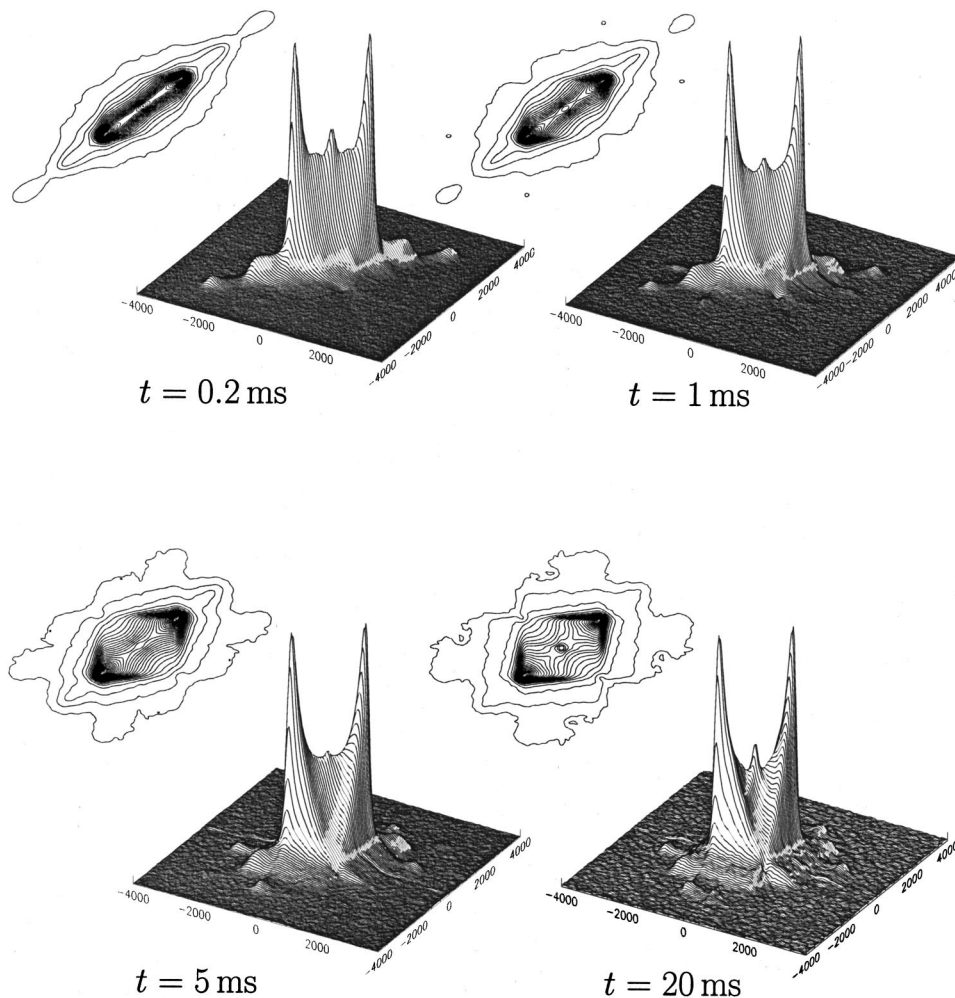


FIG. 5. ^2H exchange spectra of MO/23 wt% $^2\text{H}_2\text{O}$ (sample no. 3) taken at 270 K (L_α phase) at different mixing times t .

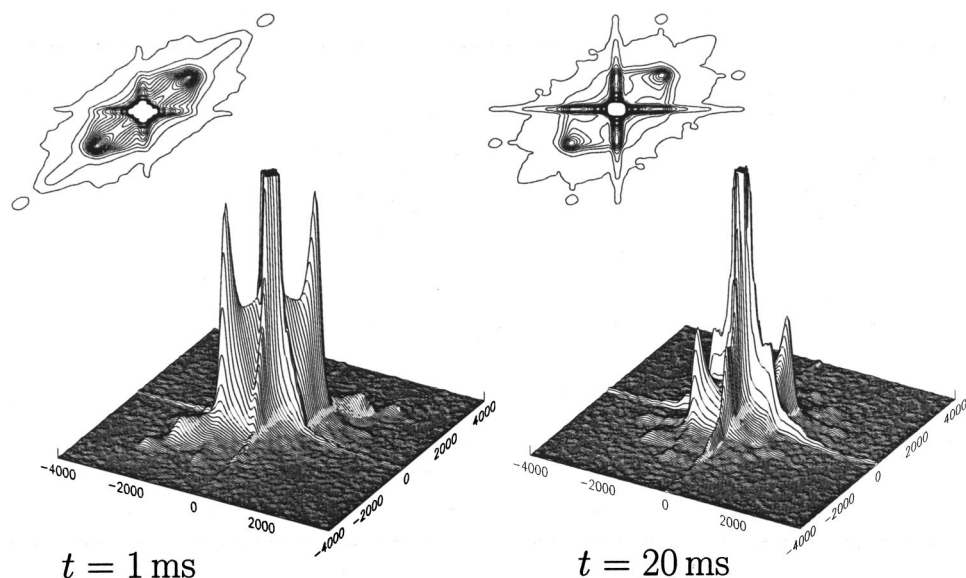


FIG. 6. ^2H exchange spectra and corresponding contour plots of MO/23 wt% $^2\text{H}_2\text{O}$ (sample no. 3) at 284 K (coexistence regime of the L_α —and Q_{II}^G —phases) at two mixing times t .

(small-angle) reorientation mechanisms. This rotational diffusion of the membrane director can be understood in terms of Sec. II B if the translational diffusion of the water deuterons is restricted to 2D layers in between a *smoothly curved* membrane stack. Thus, the reorientation of the membrane director is directly caused by the translational water diffusion. Fitting this series of spectra with computer simulations of “rotational diffusion spectra” allows one to estimate a correlation time $\tau_D \cong 2$ ms. Together with a rough extrapolation of the translational water diffusion coefficient $D_0 \cong 10^{-10} \text{ m}^2 \text{ s}^{-1}$ —using the fast deuteron component in the MO/water system, Fig. 6 of Ref. [1]—we obtain a mean lamella curvature radius of $\langle r^2 \rangle^{1/2} \cong (4D_0\tau_D)^{1/2} \cong 1 \mu\text{m}$.

A closer look at the outer parts of these spectra, where the lipid headgroup deuteron intensity is found, reveals an additional weak but distinct exchange between both deuteron species, best visible in the cross section area of the two Pake spectrum singularities. From the time evolution of these cross section intensities we can estimate a mean residence time of the deuterons at the lipid headgroup site of about 5 ms.

A second series of 2D exchange spectra was taken in the two-phase regime between the lamellar and the cubic phases

(Fig. 6). Again, the short time spectrum is restricted to the principal diagonal axis and reveals the corresponding 1D spectrum in Fig. 3. The overall line shape is a superposition of a (narrow) Pake spectrum (powder average of the membrane director of the lamellar phase) with a liquidlike contribution (arising from the deuterons in the cubic phase). Even at the $t = 1$ ms spectrum in Fig. 6 we observe a characteristic crosslike exchange pattern which becomes the dominant contribution in the spectrum at $t = 20$ ms. If we assign some 10 ms as a correlation time for this exchange process, we can again use the translational water diffusion coefficient to map the diffusion length $\langle r^2 \rangle^{1/2} \cong (4D_0\tau_D)^{1/2}$ onto an average domain size in this heterogeneous two-phase regime of approximately $5 \mu\text{m}$.

Finally, we turn to the hexagonal phase spectra (Fig. 7). In contrast to the other cases just mentioned, we do not see off-diagonal intensity up to a few hundred ms. In the picture developed above, one must assume that the translational diffusion of the water molecules is restricted to regions of constant tube director for at least more than 600 ms. Again mapping the diffusion times on a length scale, one must conclude that the water molecules are found inside noncurved “pipes”

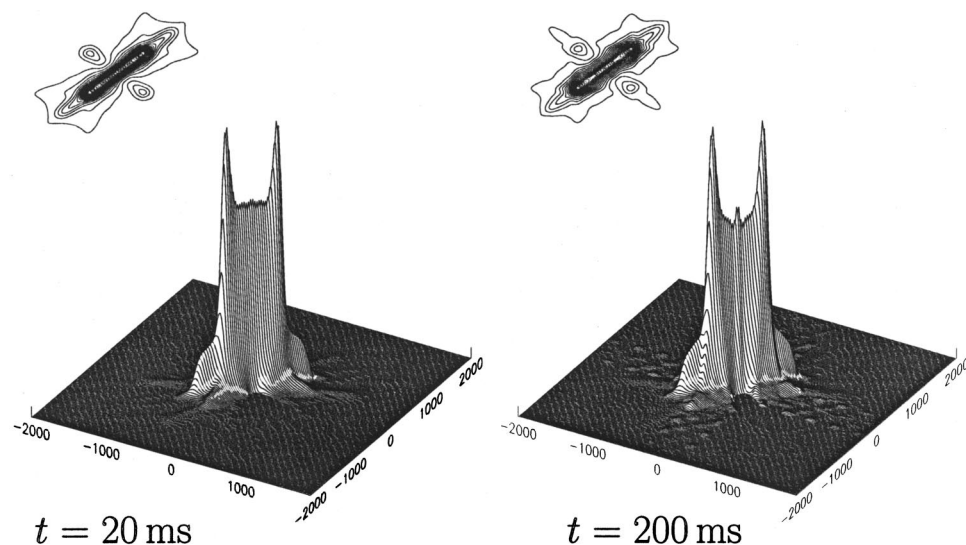


FIG. 7. ^2H exchange spectra and corresponding contour plots of MO/23 wt% $^2\text{H}_2\text{O}$ (sample no. 3) at 350 K (hexagonal phase H_{II}) at two mixing times t .

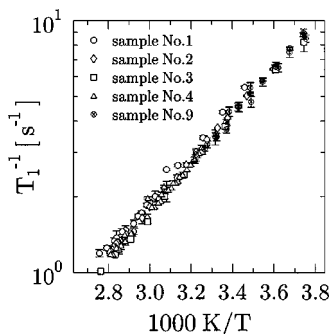


FIG. 8. Temperature dependence of ^1H spin-lattice relaxation rates of lipid molecules in MO/water dispersions at different levels of hydration.

of lengths not below some $10\ \mu\text{m}$. At first sight this result represents a contradiction to our previous diffusion data [1], as summarized in Sec. I. On the other hand, the outcomes of both experiments are reliable enough (and have been verified by many careful experiments) that we need to find a structural model that can explain translational correlation times that are much shorter than the corresponding reorientational correlation times. Developing such a model will require further experimental data and is far beyond the goal of this paper.

Note that all time scales obtained from the time evolution of 2D spectra should be considered very rough estimates. Future investigations performed in the time domain [13] should generate more quantitative numbers for these exchange processes.

B. Spin-lattice relaxation rates

In addition to the study of slow modes, i.e., translational diffusion [1] and rotational dynamics (Sec. III A), we present spin-lattice relaxation rates on both lipids (^1H -NMR) and water (^2H -NMR). Spin-lattice relaxation, being insensitive to diffusion along mesoscopically scaled curved surfaces, is a truly local probe. Since our work does not seek an understanding of fast local molecular dynamics, we will not attempt to interpret absolute relaxation rates. Instead, we are pursuing the question of to what extent spin-lattice relaxation rates reflect the interaction between water and lipids. An important control parameter for such a study is given by the relative amount of hydration. Because of the fast exchange of the water molecules between lipid surface sites and liquid bulk sites, the spin-lattice relaxation rate is expected to be hydration dependent only for water but not for the lipids that reside in monomolecular “sheets” placed at the surface of the water channels/layers.

1. Monoolein

Figure 8 shows T -dependent ^1H spin-lattice relaxation rates for several differently hydrated samples. (The measurements have been carried out in parallel with the diffusion data [1] in a magnetic field of 1.2 T and a field gradient of 22.4 T/m.) It is obvious from the figure that in the entire covered temperature range the relaxation is governed by just one thermally activated process which is not altered by a phase change. Further, we find within our experimental accuracy that the rates are essentially independent of the water

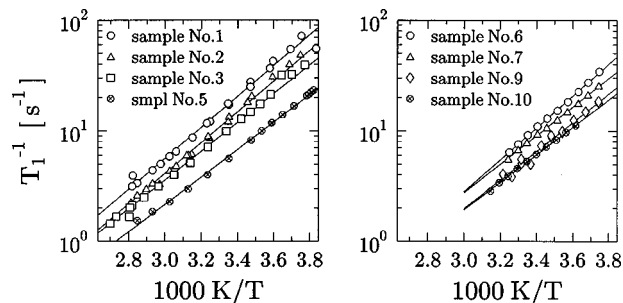


FIG. 9. Temperature dependence of ^2H spin-lattice relaxation rates of water in samples of batch 1 (left) and batch 2 (right).

content. All of these results are reasonable and in harmony with the literature [14], and we can thus safely assume that the spectral density at a frequency as high as the Larmor frequency of about 53 MHz is essentially given by fast lipid rotations about the principal molecular axis. Also, the observation that phase transitions, i.e., different local topologies, in particular between fluid mesophases, have no influence on the local lipid dynamics has been pointed out for other amphiphil-water systems [15]. The hydration independence supports our previous [1] conclusion that even in the sample with the lowest water content (sample no. 1, three water molecules per lipid), the membrane is fully hydrated. The activation energies for all samples scatter around 18 kJ/mol with a high relative precision of about 1%. A comparison with activation energies obtained from lateral diffusion coefficients [1] is misleading since, as already suggested above, the underlying processes might be different from each other. Finally, we wish to state that the relaxation curves are essentially monoexponential. Slight but systematic deviations from monoexponentiality in the cubic phase, parametrized by a Kohlrausch stretching parameter of 0.90 ± 0.03 , may be due to either inherent inhomogeneities or a mobility gradient along the lipid acyl chain [16]. We leave this question unresolved in our present context. We will perform detailed field-cycling experiments in the future.

2. Water

The measured ^2H relaxation rates (Fig. 9) yield analogous information about water dynamics. Here, we find systematic discrepancies between the two batches. The rates of batch 2 turn out to be systematically smaller than those of batch 1. Since this kind of systematics is not found in the ^2H spectra, we assign this systematic shift to paramagnetic impurities, e.g., incomplete oxygen degassing, which differ among the two batches. What is relevant for our present purpose, how-

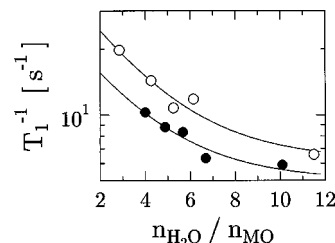


FIG. 10. Hydration dependence of ^2H spin-lattice relaxation rates at 295 K. Open symbols, batch 1; solid symbols, batch 2. Lines are fits of the Volke hydration model [17] to the data.

ever, is a trend within each batch towards lower rates with increasing level of hydration. This trend consistently appears in both batches (Fig. 10). We will return to this remarkable trend in the discussion below. Moreover, we note that (like the lipid relaxation) the water relaxation rates are insensitive to phase transitions. The temperature dependence of the rates can again be described by a simple Arrhenius behavior with activation energies that gradually decrease from 28 kJ/mol to 24 kJ/mol as the hydration is increased from about 3 to 12 $^2\text{H}_2\text{O}$ molecules per lipid. The activation energies do not show any systematic deviations between the two batches. Finally, we note that according to our expectations the measured ^2H relaxation curves have always been monoexponential.

IV. DISCUSSION

In this section we will not only discuss the above presented spectra and relaxation rates, but also take up again the diffusion coefficients dealt with in our previous paper [1]. Our goal is to arrive at a unified understanding of the three observables—diffusion, spectra, and relaxation rates—thus focusing on two key properties, namely obstruction and hydration. Obviously, this has already been done at several instances in our first paper [1] and in the preceding sections.

Let us therefore very briefly summarize, in terms of a few key words, where obstruction effects have been seen so far.

(1) Lipid diffusion coefficients “jump” when the system undergoes a phase transition from a cubic to a hexagonal phase.

(2) In both the lamellar and the hexagonal phases, ^2H 1D water spectra retain, according to the system’s phase state, some well defined anisotropy. On a longer time scale, 2D spectral shapes further reflect the curved mesostructures of these topologies.

We summarize as well where hydration effects have been noticed.

(1) There is a slow ^2H exchange between water and the lipid headgroups.

(2) The effective water diffusion coefficient increases with the level of hydration.

(3) The width of ^2H spectra slightly decreases with the hydration level.

(4) So does the ^2H relaxation rate.

Let us, in the following, look at both obstruction and hydration effects more closely and quantitatively. Emphasis will be placed on the hydration dependence of our results. The discussion will include the diffusion data published in our previous paper [1].

A. Obstruction effects

Even if locally lipid diffusion differs from water diffusion in its dimensionality, both look the same on a mesoscopic length scale as it is accessed by gradient NMR [1]. Thus, translational dynamics of *both* components can be treated as free 1D (H_{\parallel} -phase) and 2D (L_{α} -phase) dynamics and as quasi-free 3D dynamics in the cubic phases. In all cases, the boundaries can be considered as impenetrable barriers, since finite permeabilities are not relevant in our time range [18,19].

Free 1D (along a tube, director parallel to tube axis) and 2D

(within in a plane, director normal to plane) diffusion is described by a diffusion tensor [20]

$$D = \begin{pmatrix} D_{\perp} & 0 & 0 \\ 0 & D_{\perp} & 0 \\ 0 & 0 & D_{\parallel} \end{pmatrix}, \quad (10)$$

with D_{\parallel} and D_{\perp} denoting the diffusion coefficients along the director and perpendicular to the director, respectively. In dealing with powdered samples we must distinguish between two cases, inhomogeneous and homogeneous averaging. In the inhomogeneous case, where the diffusing particle does not leave its crystallite and/or where the director orientation does not vary during the experimental NMR evolution time, the gradient echo decay curves consist of a sum to which all director orientations contribute. This results in a distinct non-Gaussian-shaped echo decay curve. In the MO/ H_2O system, however, the experiments carried out in the H_{\parallel} phase verify the homogeneous scenario [1]. In this case, the molecules, both lipid and water, average over all orientations, resulting in an effective diffusion coefficient.

(a) 1D diffusion (H_{\parallel} phase):

$$D_{\perp} = 0; \quad D_{\text{eff}} = \frac{1}{3} \text{Tr}(D) = \frac{1}{3} D_{\parallel}. \quad (11a)$$

(b) 2D diffusion (L_{α} phase):

$$D_{\parallel} = 0; \quad D_{\text{eff}} = \frac{1}{3} \text{Tr}(D) = \frac{2}{3} D_{\perp}. \quad (11b)$$

In many cases, D_{\parallel} and D_{\perp} can be identified with the local diffusion coefficient D_0 . The reduction factor, $\frac{1}{3}$ in the hexagonal phase and $\frac{2}{3}$ in the lamellar phase, is commonly called an “obstruction factor,” denoted by λ (λ_H and λ_L , respectively).

Translational dynamics within the bicontinuous cubic phases are much more difficult to quantify in terms of diffusion coefficients. Again, for long observation times the trajectory of the diffusing particle averages over the local topology, thus leading to an effective diffusion coefficient.

$$D_{\text{eff}} = \lambda_C D_0. \quad (11')$$

The obstruction factor λ_C is again a measure of the reduction of the diffusion coefficient and depends on details of the topology of the phase under consideration [21,22]. In most cases, however, λ_C cannot be determined analytically. In the Appendix we present our numerical simulations of a discrete random-walk model, which includes information already known from literature and from the few existing analytical solutions. The most important results are as follows: For both lipids and water, the obstruction factor gradually decreases from $\frac{2}{3}$ towards $\frac{1}{3}$ as the lipid volume fraction is increased (Fig. 14, Appendix).

Figure 11 is a summarizing plot of the lipid diffusion data from our previous work [1]. We can now understand all (present and absent) features. The observed sudden reduction in D_{eff} at the phase transition from the Q_{\parallel}^G to the H_{\parallel} phase is easily rationalized. In the hydration range of the samples in this study (lipid volume ratio $\Phi_L \in [0.61, 0.86]$) the obstruction factor in the cubic phase is about $\lambda_C \cong 0.45 \cdots 0.5$. In the hexagonal phase we have $\lambda_H = \frac{1}{3}$. Thus, we can expect—in

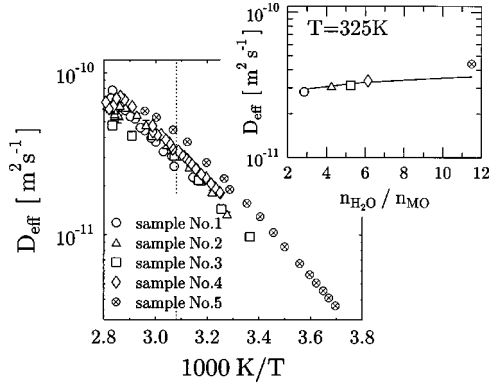


FIG. 11. Summarizing representation of lipid diffusion data (taken from Ref. [1]) of MO/water dispersions (sample nos. 1 to 5). Upper right: hydration dependence of interpolated diffusion coefficients at 325 K [dashed line in the $D_{\text{eff}}(T)$ plot]. Solid line denotes the expectation due to obstruction effects; see text.

accordance with the experiment—a reduction by a factor of $(\lambda_C - \lambda_H)/\lambda_C \cong 0.3$ which slightly increases with hydration. We also understand the absence of a jump in the diffusion coefficient at the transition between two cubic phases: The corresponding obstruction factors do not change.

Diffusion data interpolated from five samples at a selected temperature are also plotted versus the hydration level (Fig. 11, upper right) and compared to the curve expected from the water concentration dependence of the obstruction factor. We note that the observed behavior can indeed be traced back to obstruction effects.

If we perform the same analysis on the fast-diffusing water component (Fig. 12, data again taken from Ref. [1]) and compare the concentration dependence of the diffusion coefficient with the expected behavior due to obstruction effects (Fig. 12, upper right, dotted line), we note a pronounced disagreement. Obstruction effects *do not* account for the observed concentration dependence of the effective water diffusivity.

B. Hydration effects

One hydration effect already previously described [1] is the tendency that with increasing hydration, the water diffu-

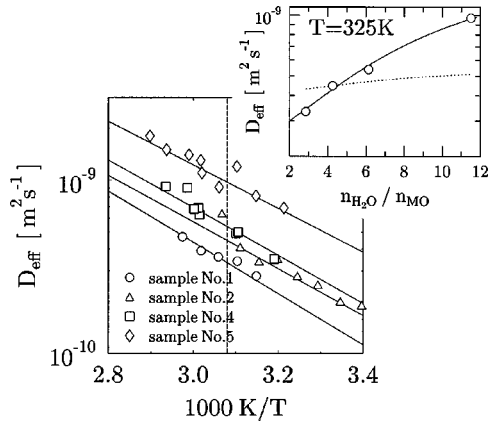


FIG. 12. Temperature dependence of the water diffusion coefficients of MO/ $^2\text{H}_2\text{O}$ taken from [1]. Upper right: experimental hydration dependence at 325 K; that of the simulated obstruction effect is indicated by the dotted line, the hydration effect due to the Volke model [17] by the solid line.

sion coefficient activation energy converges toward that of pure $^2\text{H}_2\text{O}$, which is 18.2(6) kJ/mol. At the other edge, for decreasing hydration the value for diffusive lipid dynamics (of about 32 kJ/mol) is approached. A close correlation of the dynamics of the water molecules with the translational dynamics of the lipids at these low levels of hydration is found in other lipid dispersions as well [23].

The strong concentration dependence of water diffusion qualitatively anticipates the conclusions of the following discussion: The data can be best understood if we assume rapidly exchanging lipid hydration shells. Such models are widespread in the literature, ranging from the models of two rapidly exchanging water components [24,25] to those of a gradual decreasing interaction between the lipid surface and the water molecules as their distance to the surface increases [26,27,17].

Let us demonstrate the relevance of such models by applying the approach of Volke *et al.* [17] which, as we will see, explains not only the hydration effect on the effective water diffusion coefficients but also that of the residual water ^2H quadrupole splittings in the anisotropic phases and that of the water ^2H spin-lattice relaxation rates.

(a) *Water diffusion coefficients.* Within the NMR time scale, each water molecule traverses many unit cells such that we can safely assume that it also averages over all distances from the lipid surface. The control parameter of the Volke model is the number n of water molecules per lipid, $n = n_{\text{H}_2\text{O}}/n_{\text{MO}}$. This number n can be considered a measure for the (exponentially) decreasing influence of the lipid membrane on the water dynamics. Volke introduces two more adjustable parameters, a decay constant $N_{c,d}$ of the surface influence ($N_{c,d}$ can be interpreted as the number of slow water molecules per lipid) and a ratio $f_\tau = \tau_s^0/\tau_f$ of correlation times of the slow (strongly interacting) water τ_s^0 and fast (bulk) water τ_f . With D_f denoting the known bulk water diffusion coefficient, the effective water diffusion coefficient is then derived as

$$D = D_f + \frac{N_{c,d}}{n} D_f \ln \left[\frac{1 + f_\tau e^{-n/N_{c,d}}}{1 + f_\tau} \right]. \quad (12)$$

A fit of the data in the (upper right) inset of Fig. 12 with Eq. (12) is plotted as a solid line. The fitted number $N_{c,d} = 2.7(3)$ of strongly interacting water molecules per MO, the correlation time of which is increased by a factor of $f_\tau = 5.6(5)$, is in good agreement with results obtained from phospholipid membranes [17].

(b) *Residual quadrupole coupling constants.* As can be seen from Fig. 13, the hydration dependence of the ^2H spectral widths (frequency splitting between the two Pake singularities) in the anisotropic phases diminishes, i.e., the influence of the surface on an average water molecule gets smaller with increasing hydration. From the viewpoint of the Volke model [17], the residual quadrupole splitting, $\Delta\nu_q$, is reduced with respect to the (hypothetical) splitting at vanishing degree of hydration, $\Delta\nu_q^0$, according to

$$\Delta\nu_q = \frac{1}{n} \Delta\nu_q^0 N_{c,q} (1 - e^{-n/N_{c,q}}). \quad (13)$$

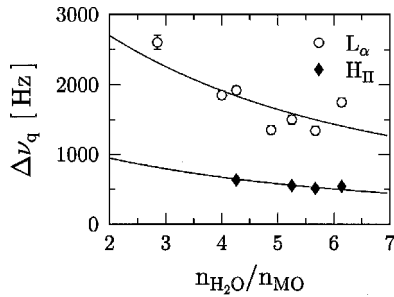


FIG. 13. Hydration dependence of the residual quadrupole coupling constant of the water deuterons in the lamellar and hexagonal phases. Solid lines represent the Volke hydration model [17].

A simultaneous fit of Eq. (13) to the data from both the lamellar and hexagonal phases yields an (at least qualitatively) reasonable result. The fitted value of $N_{c,q} = 2.3(1.3)$ turns out to be consistent with $N_{c,d}$ gained from the water diffusion data.

(c) *Spin-lattice relaxation rates.* A hydration dependence of the ^2H water relaxation rates has already been noted from inspection of Fig. 9. Also for this observable the Volke model [17] offers a prediction, namely,

$$\frac{1}{T_1} \sim [\tau_S^0 e^{-n/N_{c,r}} + \tau_f(1 - e^{-n/N_{c,r}})]. \quad (14)$$

Again, the experimental data have been fitted with Eq. (14) under the assumption that—regardless of the shift in the absolute rates of the two batches (cf. Sec. III B 2)—the hydration dependences in the two batches are identical. A simultaneous fit of the two data sets (Fig. 10) then yields for the number of closely attached water molecules (per MO) $N_{c,r} = 2.8(1.2)$, a value which is in excellent agreement with its counterparts $N_{c,d}$ (diffusion) and $N_{c,q}$ (quadrupole spectra).

V. CONCLUSIONS

This work is the direct extension of previous work [1] on translational diffusion of water and lipid molecules in MO/H₂O mesophases. The richness of this work stems from the *combination* of three different NMR methods: diffusion, spectroscopy, and relaxation. The analysis of our previous gradient NMR diffusion data is improved by interpreting them in terms of obstruction effects in the mesophases under study. In particular, the jumplike change of the lipid diffusion coefficient at the transition from the Q_{II}^G to the H_{II} phase as well as the hydration dependence of diffusion can be perfectly understood by comparison with numerical results. The same holds for the hydration effect of the diffusivity. In contrast to the lipids, water diffusion cannot be understood in terms of obstruction effects alone. Here, the pure topological effects are screened by the water-lipid surface interactions. The hydration dependence of the diffusion constant can be understood in terms of a fast exchange of molecules between a surface layer and a more bulklike volume. If we go beyond such a bimodal model and interpret the data in terms of an exponentially decreasing influence of the surface on the water dynamics, we arrive at about two to three strongly interacting water molecules per MO. Here we avoid the term “bound” (which reflects too much on the two-state model)

in favor of “strongly interacting.” Still, this latter term should not be misinterpreted, since from our data we deduce a slowing down of the molecules close to the surface only by roughly a factor of 5 as compared to bulk water molecules.

Deuteron spectroscopy shows close correlations between the (an)isotropy of topology and spectra. In the lamellar phase, the existence of two subspectra supports the previously seen [1] evidence of a slow (ms range) deuteron exchange between water and the lipid headgroup. From the temperature dependence of the residual quadrupole splitting, we can confer on a headgroup mobility that strongly increases with temperature and, analyzing its concentration dependence in terms of hydration layers, we obtain further support for the existence of two to three water molecules per MO that strongly interact with the lipid surface. The number is well supported by the exceptional behavior of the water dynamics in the lowest hydrated sample (sample no. 1, which, by preparation, contains ≈ 3 water molecules per MO). Here, the 1D spectra unambiguously show that the water dynamics is strongly coupled to the lipid headgroup dynamics.

Two-dimensional deuteron exchange spectroscopy yields evidence that in the lamellar phase the water molecules diffuse along the membranes which are curved with a mean curvature radius of the order of one μm . In the region of coexistence of lamellar and cubic phases, the domain sizes can be estimated from 2D exchange spectra to measure a few μm . In the hexagonal phase no spectral exchange is found, which sets a lower bound for a correlation length of the water tubes of about 10 μm . This remains in contradiction to MO diffusion results [1], which set an upper domain size limit of about 1 μm .

Spin-lattice relaxation probes local processes. Therefore, in our present context we discard the absolute relaxation rates. From the temperature and hydration dependences, however, we obtain valuable information complementing and supporting some previous results. The MO relaxation shows essentially no dependence on the water content. On the other hand, the water relaxation rates are much more sensitive to the degree of hydration and support the above scheme of a strong water-surface interaction which involves some two to three water molecules per MO.

VI. OPEN QUESTIONS AND FURTHER OUTLOOK

We are left with a couple of open questions, the most serious one of which concerns the apparent contradiction between diffusion and 2D spectral data on the tube correlation length in the H_{II} phases. There are two possible pathways out of this dilemma. In one of the measurements (on sample no. 2) a pronounced orientation occurred in the hexagonal phase which was absent in a (one year) earlier measurement on the same sample. This is inferred from the clear tendency of the deuteron spectra to change from a Pake-like shape toward a linelike shape. These spectral changes are to be interpreted in terms of a macroscopic tube director orientation parallel to the external magnetic field. It is unclear to date whether aging effects or just the sample thermal history just before reaching the hexagonal phase is responsible for this nonreproducibility. The second observation has been the drastic reduction (of about 30 K) of the phase transition temperature

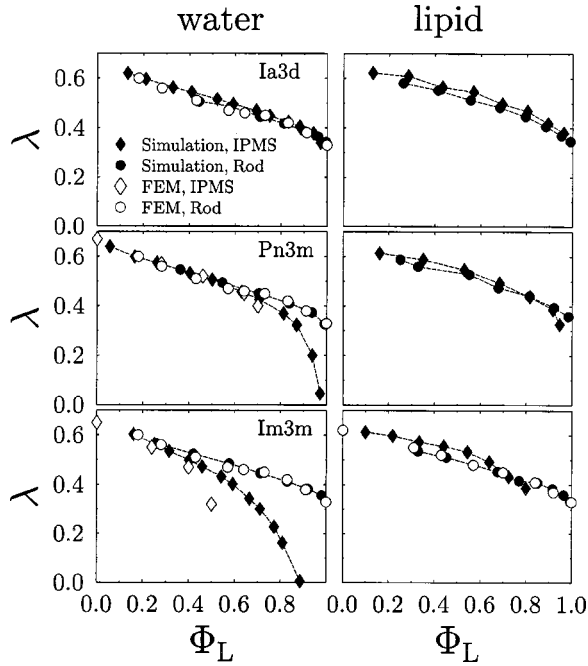


FIG. 14. Obstruction factors resulting from random-walk simulations of water (left side) and lipid (right side) in cubic topologies as a function of lipid concentration. For comparison, literature data from finite element calculations are also shown [22]. Lines are guides to the eyes.

$T(Q_{\parallel}^G \rightarrow H_{\parallel})$ of the sample inside a magnetic field as compared to the calorimetry (zero field) value. In any case, the phase behavior seems to be correlated with the applied magnetic field. In fact, correlations of this kind are known, e.g., from liquid-crystalline nematic phases [28]. Here, diffusion and spectral measurements in different magnetic fields are needed.

Higher magnetic fields may also be useful in another application. For intensity reasons, so far water diffusion ($^2\text{H NMR}$) experiments have had to be restricted to Hahn echo decays. What would really be desirable is stimulated echo data. Such experiments in the stray field of a very high field magnet are planned.

As far as deuteron exchange spectroscopy in the anisotropic phases is concerned, we have so far only looked at 2D spectra at a few selected mixing times. This allowed us to estimate correlation times, but no more. We know from our own experience [13] that 2D echos in the time domain will take us much further in determining the geometric and temporal characteristics of the water dynamics along curved surfaces. Such experiments are very time consuming and represent a separate project.

We have addressed spin-lattice relaxation rates but have avoided the interpretation of absolute rates. Presently, as stated, we are working on a field-cycling spectrometer that will be of use in determining the local modes.

Finally, let us mention our desire to perform quasielastic neutron scattering experiments to learn about the *local* water diffusion coefficient. Unfortunately, the most straightforward way of proceeding, which would be the screening of the lipid by deuteration, is an extremely difficult task in the case of MO. We would have to separate the scattered intensity con-

tributions of the diverse components, a possible but not easy task.

ACKNOWLEDGMENT

This work has been carried out at the Universität Dortmund within the framework of the DFG-Graduiertenkolleg ‘‘Struktur-Dynamik-Beziehungen in mikrostrukturierten Systemen.’’

APPENDIX: RANDOM WALKS AND OBSTRUCTION FACTORS

Principally, the obstruction factors describing the quasi-free three-dimensional diffusion of lipid and water molecules in cubic topologies may be obtained by solving the diffusion equation

$$P(\vec{r}, t) \frac{\partial}{\partial t} = D \Delta P(\vec{r}, t) \quad (\text{A1})$$

with appropriate boundary conditions. But only a few special cases allow for analytical solutions; all others call for numerical methods. In the literature, the method of finite elements has been used to obtain obstruction factors for some of the topologies under consideration here [22]. Our approach is based on random-walk simulations. We will present results for the restricted diffusion of water molecules and the surface diffusion of lipid molecules in the context of two models for the $Im3m$, $Pn3m$, and $Ia3d$ cubic phases.

The interconnected rod model [29] assumes that the water component is restricted within tubes of equal length that assemble bicontinuous networks of simple cubic ($Im3m$), diamond ($Pn3m$), and Laves ($Ia3d$) type [30]. The tubes are bounded by lipid molecules with the hydrophilic headgroup oriented towards the water. Today, infinite periodic minimal surfaces (IPMS) are most often used to describe lyotropic cubic phases [31]. Within this model, the ends of the hydrophobic chain meet at the Schwarz primitive ($Im3m$) or diamond ($Pn3m$) surface [32], or at the Schoen gyroid surface ($Ia3d$) [33].

Before turning to the simulations, we will consider available analytical results. Anderson and Wennerstrom have shown that the obstruction factor of lipid molecules for the $Im3m$ -IPMS model in the limit of vanishing lipid content ($\Phi_L \rightarrow 0$) is $\frac{2}{3}$. A semiquantitative solution for the water diffusion in the case ($\Phi_L \rightarrow 1$) in the interconnected rod model of each of the three cubic phases may be obtained as follows. The diffusion path of a water molecule consists of connected tubes (diameter small compared to their length d) and may be written as

$$\vec{R} = \sum_{i=1}^n \vec{r}_i, \quad (\text{A2})$$

which gives a mean-square displacement of

$$\langle \vec{R}^2 \rangle = \sum_{i=1}^n \langle \vec{r}_i^2 \rangle = n d^2. \quad (\text{A3})$$

The cross terms equal zero since for the m base vectors of each of the three labyrinths the equation $\sum_{i=1}^m \vec{r}_i = 0$ holds. It

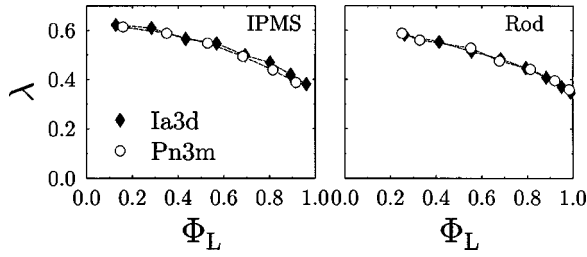


FIG. 15. Comparison of lipid obstruction factors in *Ia3d* and *Pn3m* topologies.

takes the mean time $t_1 = d^2/2D_0$ to diffuse through a single one-dimensional tube with the local diffusion coefficient D_0 . For the whole path of n tubes, we then find

$$\langle \bar{R}^2 \rangle = 6D_{\text{eff}}t, \quad (\text{A4})$$

with the effective diffusion coefficient $D_{\text{eff}} = \frac{1}{3}D_0$ and the obstruction factor $\lambda = \frac{1}{3}$.

1. Principles of random walks

The basic principle of a random walk is the approximation of the continuous diffusive motion as a discrete hopping process governed by the master equation

$$P(\vec{l}, t | \vec{0}, 0) / \frac{\partial}{\partial t} = \Gamma \sum_{\vec{l}'} [P(\vec{l}', t | \vec{0}, 0) - P(\vec{l}, t | \vec{0}, 0)]. \quad (\text{A5})$$

$P(\vec{l}, t | \vec{0}, 0)$ denotes the conditional probability of finding a walker at position \vec{l} and time t if it has been at the coordinate $\vec{r} = \vec{0}$ at $t = 0$, Γ denotes the transition probability, and the sum runs over all neighboring positions [34,35]. In general, the simulation runs on a cubic lattice, which models the appropriate boundary conditions by allowing the walker to move only on selected fields. Since the simulation is realized as a computer program, the evaluation of the mean-square displacement averaged over an ensemble of such walkers is rather simple. From this, the obstruction factor $\lambda = \langle \bar{R}^2 \rangle / 6D_0t$ with local diffusion coefficient $D_0 = \Gamma a^2$, step length a and step number t may be directly obtained.

There are two important points concerning the implementation of random-walk algorithms. First, an appropriate random number generator has to be chosen. We employ the one invented by L'Ecuyer [36]. The more critical point is the strategy of moving a walker when it approaches a boundary, especially if the ratio of surface to volume gets large. Here, it is necessary to distinguish between the three-dimensional volume diffusion of water molecules and the two-dimensional surface diffusion of the lipid. For the water diffusion, we have run test simulations with several walk strategies in selected labyrinth types (tubes and sheets of different width and oriented in several directions) whose obstruction factors are known ($\frac{1}{3}$ for tubes, $\frac{2}{3}$ for sheets independent of width and orientation). The algorithm that shows the best results with deviations of less than 5% runs as follows:

- (1) choose one of the six neighbor fields at random;
- (2) if that field is accessible, move the walker; finished;

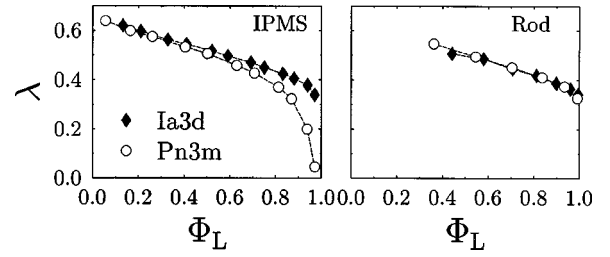


FIG. 16. Comparison of water obstruction factors in *Ia3d* and *Pn3m* topologies.

(3) if it is not, see if the field in the opposite direction is accessible;

(4) if it is, move the walker; finished;

(5) if it is not, do not move the walker at all; finished.

The two-dimensional lipid diffusion is modeled by the following strategy:

(1) choose a random vector on a unit sphere;

(2) if a move in that direction ends on an accessible field, move walker; finished;

(3) if not, repeat step 1.

Again, test simulations have been successfully performed on sheets and tube surfaces with a width of one field.

2. Simulations

All simulations are performed with 10 000 walkers and at least 100 000 steps in labyrinths of size $150 \times 150 \times 150$ for volume and $200 \times 200 \times 200$ for surface diffusion. As expected, all data show a linear relationship between $\langle \bar{R}^2 \rangle$ and t , allowing the direct determination of the effective diffusion coefficient and the obstruction factor.

Figure 14 shows the results of our simulations as well as data from the literature for comparison. With the exception of water diffusion in the *Im3m*-IPMS labyrinth, they are in good agreement. The observed deviation may be due to the finer discretization of the random-walk labyrinths, which affects the concentration level where bottlenecks begin to play a role. Both analytical results, an obstruction factor of $\frac{2}{3}$ for lipid diffusion in the *Im3m*-IPMS labyrinth at high water content and $\frac{1}{3}$ for water diffusion in interconnected-rod labyrinths at low water content, are obtained numerically.

Only the water diffusion in *Im3m* and *Pn3m* phases exhibits a dependence on the chosen labyrinth model. This also is an effect of the previously mentioned bottlenecks, which may by definition only occur in the IPMS model.

In further data analysis, we concentrate on the two cubic phases relevant to the monoolein-water system, namely, the *Pn3m* and the *Ia3d* phases. We investigate whether a transformation between these topologies may be observed experimentally by diffusion measurements. From Fig. 15 it becomes obvious that the obstruction factors of lipid diffusion are independent of the phase for both labyrinth models. This implies that we cannot expect to observe a change in the system topology in lipid diffusion coefficients. Figure 16 indicates that this is also true for water diffusion in interconnected-rod labyrinths. Only in the limit of very low water content and within the IPMS model do the water obstruction factors of the *Pn3m* and *Ia3d* phases differ and possibly allow the identification of a phase transition.

- [1] B. Geil, T. Feiweier, E.-M. Pospiech, J. Eisenblätter, F. Fujara, and R. Winter, *Chem. Phys. Lipids* **106**, 115 (2000).
- [2] S. T. Hyde and S. Anderson, *Z. Kristallogr.* **168**, 213 (1984).
- [3] J. Briggs, H. Chung, and M. Caffrey, *J. Phys. II* **6**, 723 (1996).
- [4] C. Czeslik, R. Winter, G. Rapp, and K. Bartels, *Biophys. J.* **68**, 1423 (1995).
- [5] E. Lang and H.-D. Lüdemann, *Ber. Bunsenges. Phys. Chem.* **84**, 462 (1980).
- [6] K. Schmidt-Rohr and H. W. Spiess, *Multidimensional Solid-State NMR and Polymers* (Academic, London, 1994).
- [7] J. H. Davis, K. R. Jeffrey, M. Bloom, and M. I. Valic, *Chem. Phys. Lett.* **42**, 390 (1976).
- [8] J. Charvolin and P. Rigny, *J. Phys. (France)* **30**, C4-76 (1969).
- [9] H. Sillescu, *J. Chem. Phys.* **54**, 2110 (1971).
- [10] S. Wefing, S. Kaufmann, and H. W. Spiess, *J. Chem. Phys.* **89**, 1234 (1988).
- [11] A. Pampel, E. Strandberg, G. Lindblom, and F. Volke, *Chem. Phys. Lett.* **287**, 468 (1998).
- [12] A. Nilsson, A. Holmgren, and G. Lindblom, *Chem. Phys. Lipids* **71**, 119 (1994).
- [13] B. Geil, F. Fujara, and H. Sillescu, *J. Magn. Res.* **130**, 18 (1998).
- [14] P. O. Eriksson, A. Khan, and G. Lindblom, *J. Phys. Chem.* **86**, 387 (1982).
- [15] J. Charvolin and P. Rigny, *J. Chem. Phys.* **58**, 3999 (1973).
- [16] J. H. Davis, K. R. Jeffrey, and M. Bloom, *J. Magn. Res.* **29**, 191 (1978).
- [17] F. Volke, S. Eisenblätter, J. Galle, and G. Klose, *Chem. Phys. Lipids* **70**, 121 (1994).
- [18] M. Jansen and A. Blume, *Biophys. J.* **68**, 997 (1995).
- [19] A. R. Waldeck, P. W. Kuchel, A. J. Lennon, and B. E. Chapman, *Prog. Nucl. Magn. Reson. Spectrosc.* **30**, 39 (1997).
- [20] P. T. Callaghan, *Aust. J. Phys.* **37**, 359 (1984).
- [21] B. Jönsson, H. Wennerström, P. G. Nilsson, and P. Linse, *Colloid Polym. Sci.* **264**, 77 (1986).
- [22] D. M. Anderson and H. Wennerström, *J. Phys. Chem.* **94**, 8683 (1990).
- [23] P. Karakatsanis and T. M. Bayerl, *Phys. Rev. E* **54**, 1785 (1996).
- [24] P. T. Inglefield, K. A. Lindblom, and A. M. Gottlieb, *Biochim. Biophys. Acta* **419**, 196 (1976).
- [25] R. H. Walmsley and M. Sphorer, *J. Phys. Chem.* **65**, 2584 (1978).
- [26] D. E. Woessner, *J. Magn. Res.* **39**, 297 (1979).
- [27] A. S. Ulrich and A. Watts, *Biophys. Chem.* **49**, 39 (1994).
- [28] P. J. Black, K. D. Lawson, and T. J. Flautt, *Mol. Cryst. Liq. Cryst.* **7**, 201 (1969).
- [29] V. Luzatti, T. G. Krzywicki, and A. Tardieu, *Nature (London)* **218**, 1031 (1968).
- [30] H. Heesch and F. Laves, *Z. Kristallogr.* **85**, 443 (1933).
- [31] L. E. Scriven, *Nature (London)* **263**, 123 (1976).
- [32] H. A. Schwarz, *Gesammelte Mathematische Abhandlungen*, 2nd ed. (Chelsea Publishing Company, New York, 1972).
- [33] A. H. Schoen, NASA Technical Report No. D5541, 1970.
- [34] J. W. Haus and K. W. Kehr, *Phys. Rep.* **150**, 263 (1987).
- [35] K. W. Kehr, K. Mussawisade, and T. Wichmann, in *Diffusion in Condensed Matter*, edited by J. Kärgel, P. Heitjans, and R. Haberlandt (Vieweg GmbH, Braunschweig, 1998).
- [36] P. L'Ecuyer, *Commun. ACM* **31**, 742 (1988).